European Journal of Mechanics / A Solids 121 (2027) 106309

Contents lists available at ScienceDirect

European Journal of Mechanics / A Solids

journal homepage: www.elsevier.com/locate/ejmsol

Full length article

A low-frequency multimode approximation for a thin elastic sandwich

Barış Erbaş [a,b], Ludmila Prikazchikova [a,*], Julius Kaplunov [c,a]

[a] School of Computer Science and Mathematics, Keele University, Keele, ST5 5BG, UK
[b] Department of Mathematics, Eskişehir Technical University, Yunus Emre Campus, 26470, Eskişehir, Turkey
[c] Department of Continuum Mechanics, RWTH Aachen University, Kackertstraße 9, 52072, Aachen, Germany

ARTICLE INFO

Keywords:
Asymptotic
Multimode
Low frequency
High contrast
Sandwich
Dispersion

ABSTRACT

Antisymmetric low-frequency motion of a three-layered plate is considered within the framework of 3D elasticity. The skin (outer) layers are assumed to be much stiffer than the core (inner) one. The leading order 2D multimode approximation is derived. It incorporates three asymptotic behaviours, governed by bending and shear scalings as well as by a specific one related to the transition from bending to shear regimes. Dispersion of time-harmonic and evanescent waves is investigated over the frequency band involving the smallest cut-off. It is shown that the obtained polynomial expansions coincide with the long-wave low-frequency approximations of the transcendental dispersion relations arising in plane and antiplane elasticity.

1. Introduction

High-contrast sandwich plates, comprising stiff face sheets bonded to a lightweight and compliant core, are widespread in modern engineering. Their remarkable bending stiffness-to-weight ratio makes them indispensable in aerospace (Castanie et al., 2020; Yuan et al., 2012; Zhuang et al., 2021), naval (Kõrgesaar et al., 2016; Liu et al., 2022; Qiu et al., 2023), and civil (Tuwair et al., 2016; Garrido et al., 2019) structures, including aircraft fuselages, ship hulls, bridge decks, and wind turbine blades. High-contrast laminates have also been adopted in advanced glass facades (López-Aenlle and Pelayo, 2014; Boutin et al., 2021), photovoltaic modules (Aßmus et al., 2017; Schulze et al., 2012), and building insulation panels (Lee et al., 2018). Their unique dynamic characteristics have further applications in acoustic metamaterials (Martin et al., 2012; He et al., 2017) and meta-shells/plates (Smyczynski and Magnucka-Blandzi, 2018; Hohe, 2015; Singh et al., 2024), where appropriate tuning of the material contrast enables efficient wave control and vibration attenuation.

Despite their extensive industrial implementation, the mathematical modelling of high-contrast sandwich structures brings significant challenges. The large mismatch in stiffness and density between the stiff skins and the soft core gives rise to physical phenomena that do not appear in the homogeneous case. In particular, the presence of a compliant core may support additional low-frequency propagating modes as well as slowly decaying evanescent ones as follows from the multiparametric dispersion analysis in Chapman (2013), Kaplunov et al. (2017) and Prikazchikova et al. (2024). Until now, there has been no general dynamic theory capturing these effects. They were only incorporated into 1D scalar formulations recently derived for antiplane shear (Prikazchikova et al., 2020; Kaplunov et al., 2021). Thus, the derivation of mathematically consistent 2D PDEs governing the multimode vector framework is still of great demand.

Over the years, various approaches have been developed to model sandwich plates, ranging from engineering theories based on ad-hoc assumptions, e.g., see Vinson (2018) and Birman and Kardomateas (2018) and references therein, to more systematic asymptotic methods (Berdichevsky, 2010; Boutin and Viverge, 2016; Erbaş et al., 2026) mainly concerned with statics. In particular, as shown in Erbaş et al. (2026), the derived sixth-order 2D theory implies one more boundary condition due to the presence of a slowly varying boundary layer specific to high-contrast laminates. The latter was previously observed in Horgan (1998), Baxter and Horgan (1995) and Wijeyewickrema et al. (1996) when analysing the exact plane and antiplane solutions for a high-contrast semi-infinite sandwich strip.

The asymptotic approach has proven to be the most natural for thin elastic plates and shells due to the presence of a small geometric parameter, see foundational publications (Friedrichs and Dressler, 1961; Goldenveizer, 1962; Green, 1962; Goldenveizer, 1966). Nowadays, it is extended to a broad variety of boundary and initial value problems taking into account anisotropy, pre-stress, transverse inhomogeneity along with other phenomena, see, e.g., books (Kaplunov et al., 1998; Goldenveizer, 1976; Le, 2012; Aghalovyan, 2015; Rogacheva, 2020; Berdichevsky, 2009) along with journal publications (Gregory and

* Corresponding author.
E-mail addresses: b.erbas@keele.ac.uk, berbas@eskisehir.edu.tr (B. Erbaş), l.prikazchikova@keele.ac.uk (L. Prikazchikova), j.kaplunov@keele.ac.uk (J. Kaplunov).

https://doi.org/10.1016/j.euromechsol.2026.106309
Received 6 May 2026; Received in revised form 23 June 2026; Accepted 21 July 2026
Available online 27 July 2026
0997-7538/© 2026 The Authors. Published by Elsevier Masson SAS. This is an open access article under the CC BY license (http://creativecommons.org/licenses/by/4.0/).

Wan, 1984, 1985; Kaplunov et al., 2006; Pichugin and Rogerson, 2001; Wilde et al., 2022; Le, 1997; Kaplunov et al., 2022, 2000; Goldenveizer et al., 1993; Le, 2023; Aguiar et al., 2025) to mention a few. High contrast adds extra problem parameters including ratios of thicknesses, stiffnesses and densities to the asymptotic framework as illustrated, for example, by the multiparametric dispersion analysis in Kaplunov et al. (2017) resulting in a number of shortened dispersion relations depending on the ratios between contrast parameters as well as wavelength and frequency.

In this paper, we derive a 2D multimode low-frequency approximation for the antisymmetric motion of a three-layered elastic thin plate of a symmetric layout restricting ourselves to a high contrast in both stiffnesses and densities of the skin and core layers. The consideration below is based on the previous asymptotic insight into the peculiarities of dispersion phenomena, see Kaplunov et al. (2017) and Prikazchikova et al. (2024), and also (Prikazchikova et al., 2020; Kaplunov et al., 2021), treating the scalar antiplane shear deformation. From the very beginning, we aim at incorporating low-frequency plane and antiplane modes with the smallest shear cut-off frequency along with the fundamental bending mode generalizing that in the classical Kirchhoff theory for plate bending.

The derived 2D shortened equations of motion initially support two asymptotic scalings originating from bending and extension of a homogeneous plate (Kaplunov et al., 1998; Goldenveizer et al., 1993). An important feature of the considered antisymmetric motion is that extension of skins induces shear of a core. This is why throughout the paper, we refer to the last scaling as the shear one.

Merging the approximations corresponding to these two scalings into a single composite setup is achieved by adopting the idea of matched asymptotic expansions, e.g., see Kevorkian and Cole (2013), which is usually implemented for series in a small parameter rather than for differential equations. It is worth noting that the asymptotic counterpart of the classical Kirchhoff–Love shell theory (Goldenveizer, 1966, 1976) also involves two scalings corresponding to bending and membrane deformations.

It is demonstrated that the developed 2D model leads to the polynomial dispersion relations for plane and antiplane waves which are asymptotically equivalent to those derived from the associated exact transcendental equations, see Kaplunov et al. (2017, 2021), respectively. The current paper finalizes the multiparametric dispersion analysis of three propagating and evanescent waves (two plane and one antiplane) launched in previous authors' publications (Kaplunov et al., 2017; Prikazchikova et al., 2024, 2020; Kaplunov et al., 2021). The culmination is the discovery of one more asymptotic scaling, which was not assumed when deriving the established approximation. This scaling supports the transition from the bending to the shear regime for one of the plane evanescent waves.

The last observation motivated the authors to revisit the original problem implementing the spotted scaling. The related low-dimensional approximation is derived from plane-strain equations of motion. Moreover, it is shown that the latter also follows from the developed here 2D framework based on bending and shear scalings.

The paper is organized as follows. The problem is formulated in Section 2 in terms of 3D dynamic elasticity, where the key asymptotic parameters and main assumptions are introduced. The 2D equations of motion for shear and bending scalings are derived in Sections 3 and 4. The next Section 5 deals with the derivation of a composite theory using the developments of the previous two sections. The results of dispersion analysis, including, comparison with exact transcendental relations are presented in Section 6. The derivation for the additional scaling discovered in the last section is given in Appendix.

2. Problem statement

Consider a three-layered elastic plate occupying the region $-\infty < x_1, x_2 < \infty$, $-h_c - 2h_s \le x_3 \le h_c + 2h_s$. The inner core layer is defined by $-h_c \le x_3 \le h_c$ whilst the outer skin layers lie within $h_c \le |x_3| \le h_c + 2h_s$, see Fig. 1. In what follows, parameters corresponding to the core and skin layers are labelled with c and s, respectively.

The 3D equations of motion in linear elasticity are given by, e.g., see Achenbach (2012),

$$\frac{\partial \sigma_{ii}^q}{\partial x_i} + \frac{\partial \sigma_{ij}^q}{\partial x_j} + \frac{\partial \sigma_{3i}^q}{\partial x_3} - \rho_q \frac{\partial^2 v_i^q}{\partial t^2} = 0, \tag{1}$$

$$\frac{\partial \sigma_{31}^q}{\partial x_1} + \frac{\partial \sigma_{32}^q}{\partial x_2} + \frac{\partial \sigma_{33}^q}{\partial x_3} - \rho_q \frac{\partial^2 v_3^q}{\partial t^2} = 0, \tag{2}$$

where t is time, ρ_q are densities, σ_{ij}^q and σ_{3m}^q are stresses, v_m^q are displacements, $i \ne j = 1, 2$, $m = 1, 2, 3$, and $q = c, s$. The stress–displacement relations can be written in the form oriented to asymptotic analysis. They are, see Kaplunov et al. (1998) and references therein,

$$\sigma_{ii}^q = \frac{E_q}{1 - \nu_q^2}\left(\frac{\partial v_i^q}{\partial x_i} + \nu_q \frac{\partial v_j^q}{\partial x_j}\right) + \frac{\nu_q}{1 - \nu_q}\sigma_{33}^q, \tag{3}$$

$$\sigma_{ij}^q = \frac{E_q}{2(1 + \nu_q)}\left(\frac{\partial v_i^q}{\partial x_j} + \frac{\partial v_j^q}{\partial x_i}\right), \tag{4}$$

$$\frac{\partial v_3^q}{\partial x_3} = \frac{1}{E_q}\left(\sigma_{33}^q - \nu_q(\sigma_{11}^q + \sigma_{22}^q)\right), \tag{5}$$

$$\frac{\partial v_i^q}{\partial x_3} = -\frac{\partial v_3^q}{\partial x_i} + \frac{2(1 + \nu_q)}{E_q}\sigma_{3i}^q, \tag{6}$$

where E_q and ν_q are Young's moduli and Poisson's ratios.

The homogeneous boundary conditions along the faces are

$$\sigma_{3m}^s = 0 \quad \text{at} \quad x_3 = \pm(h_c + 2h_s), \tag{7}$$

whereas, at the layer interfaces, the continuity conditions take the form

$$v_m^s = v_m^c \quad \text{and} \quad \sigma_{3m}^s = \sigma_{3m}^c \quad \text{at} \quad x_3 = \pm h_c. \tag{8}$$

In this paper, we focus on a high contrast in the Young moduli and densities of the core and skin layers, assuming no contrast in thicknesses. Thus, we define the small contrast parameters

$$\varepsilon = \frac{E_c}{E_s} \ll 1 \qquad \text{and} \qquad r = \frac{\rho_c}{\rho_s} \ll 1, \tag{9}$$

setting $\varepsilon \sim r$ to handle an appropriate single parameter. This is in line with one of the scenarios considered in Kaplunov et al. (2017), which corresponds to a range of cellular-core sandwich structures (honeycomb, foams, lattice materials), characterized by large stiffness and density contrasts of the layers, see Ashby and Gibson (1997).

We also restrict ourselves to the long-wave low-frequency approximation of the formulated 3D boundary-value problem assuming that

$$\frac{h_q}{L} \ll 1 \quad \text{and} \quad \frac{h_q}{c_{2q}T} \ll 1, \tag{10}$$

where L and T are typical length and time scales, and c_{2q} denotes the shear wave speed expressed as

$$c_{2q} = \sqrt{\frac{E_q}{2\rho_q(1 + \nu_q)}}. \tag{11}$$

Here and below in this section, see Kaplunov et al. (1998) for more details. In addition, recall that $h_c \sim h_s$ and $c_{2c} \sim c_{2s}$ as follows from the assumptions above.

Our aim is to derive a multimode 2D approximation of the formulated 3D boundary-value problem under the constraints (9) and (10). In this case, we expect to incorporate both bending and shear plate motions, see Fig. 2, for which

$$L \sim \sqrt{c_{2q} h_q T} \tag{12}$$

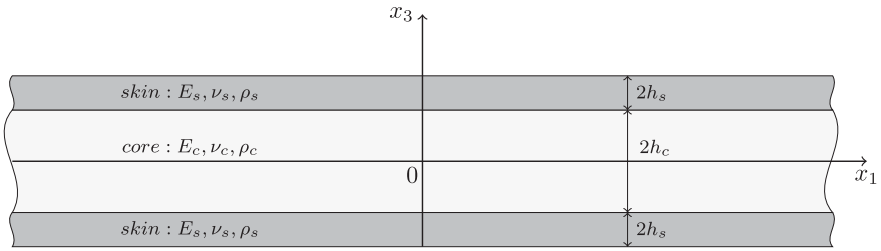

Fig. 1. A three-layered sandwich plate.

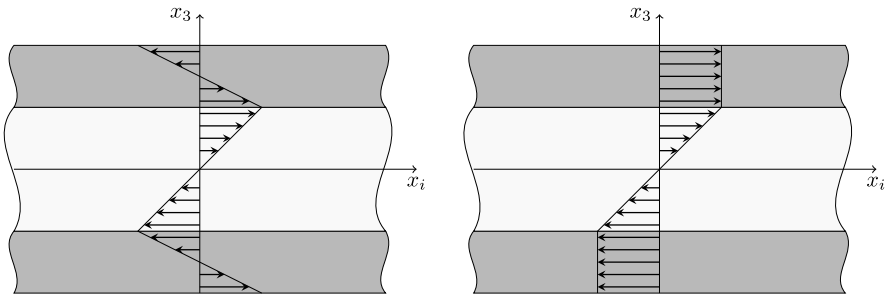

(a) Bending. (b) Shear.

Fig. 2. Variation of tangential displacements u_i, $i = 1, 2$, across the thickness for (a) bending and (b) shear motions.

and

$$L \sim c_{2q} T. \tag{13}$$

In particular, for harmonic vibrations with angular frequency ω and wavenumber k, $L \sim 1/k$ and $T \sim 1/\omega$. Then, we have from (12) and (13), respectively,

$$k \sim \sqrt{\frac{\omega}{c_{2q} h_q}} \tag{14}$$

and

$$k \sim \frac{\omega}{c_{2q}}. \tag{15}$$

All these relations are in agreement with the results of dispersion analysis in Kaplunov et al. (2017, 2021).

It can easily be verified that the second strong inequality in (10) follows from the first for each of the scalings (12) and (13). Therefore, we may operate with a small geometric parameter only, setting

$$\eta = \frac{h_c}{L} \ll 1, \tag{16}$$

where, without loss of generality, we use $q = c$ related to the core layer. Moreover, for the sake of simplicity, we suppose that $L \sim h_c/\sqrt{\epsilon}$, insuring that $L \gg h_c$. Thus,

$$\epsilon = \eta^2 E, \quad \text{and} \quad r = \eta^2 \rho, \tag{17}$$

where E and ρ are of order unity.

It is worth noting that the rationale behind the 3D → 2D reduction developed below is not limited to the clear advantages of lower-dimensional numerical modelling, but is also strongly motivated by the need for qualitative insight into novel dynamic phenomena arising from high contrast.

3. 2D shear approximation

The scaling of the independent variables supporting shear motion is given by

$$x_i = L\xi_i, \qquad x_3 = \begin{cases} h_c \zeta_c, & |x_3| \le h_c, \\ h_c + h_s(1+\zeta_s), & h_c \le |x_3| \le h_c + 2h_s, \end{cases} \tag{18}$$

and

$$t = T\tau, \tag{19}$$

with $T = L/c_{2c}$ according to the relation (13).

Consider first skin layers, dimensionalizing the displacements and stresses as

$$v_i^s = L v_i^{s*}, \quad v_3^s = h_c v_3^{s*}, \tag{20}$$

and

$$\sigma_{ii}^s = E_s \sigma_{ii}^{s*}, \quad \sigma_{ij}^s = E_s \sigma_{ij}^{s*}, \quad \sigma_{3i}^s = E_s \eta \sigma_{3i}^{s*}, \quad \sigma_{33}^s = E_s \eta^2 \sigma_{33}^{s*}. \tag{21}$$

Here and below, all starred quantities are assumed of the same asymptotic order. The adopted asymptotic set-up is the same as that in the classical theory for plane stress, see Kaplunov et al. (1998) and references therein.

Eqs. (1)–(6), rewritten in dimensionless variables and unknowns, become

$$\frac{\partial \sigma_{ii}^{s*}}{\partial \xi_i} + \frac{\partial \sigma_{ij}^{s*}}{\partial \xi_j} + \frac{1}{h}\frac{\partial \sigma_{3i}^{s*}}{\partial \zeta_s} - \frac{E}{2(1+\nu_c)\rho}\frac{\partial^2 v_i^{s*}}{\partial \tau^2} = 0, \tag{22}$$

$$\frac{\partial \sigma_{31}^{s*}}{\partial \xi_1} + \frac{\partial \sigma_{32}^{s*}}{\partial \xi_2} + \frac{1}{h}\frac{\partial \sigma_{33}^{s*}}{\partial \zeta_s} - \frac{E}{2(1+\nu_c)\rho}\frac{\partial^2 v_3^{s*}}{\partial \tau^2} = 0, \tag{23}$$

and

$$\sigma_{ii}^{s*} = \frac{1}{1-\nu_s^2}\left(\frac{\partial v_i^{s*}}{\partial \xi_i} + \nu_s \frac{\partial v_j^{s*}}{\partial \xi_j}\right) + \eta^2 \frac{\nu_s}{1-\nu_s}\sigma_{33}^{s*}, \tag{24}$$

$$\sigma_{ij}^{s*} = \frac{1}{2(1+\nu_s)}\left(\frac{\partial v_i^{s*}}{\partial \xi_j} + \frac{\partial v_j^{s*}}{\partial \xi_i}\right), \tag{25}$$

$$\frac{\partial v_3^{s*}}{\partial \zeta_s} = -h\left(\nu_s(\sigma_{11}^{s*} + \sigma_{22}^{s*}) - \eta^2 \sigma_{33}^{s*}\right), \tag{26}$$

$$\frac{\partial v_i^{s*}}{\partial \zeta_s} = -h\eta^2\left(\frac{\partial v_3^{s*}}{\partial \xi_i} - 2(1+\nu_s)\sigma_{3i}^{s*}\right), \tag{27}$$

where $h = h_s/h_c$.

Below, due to symmetry, we consider only the upper skin layer, imposing the boundary conditions (7) at $\zeta_s = 1$. They are

$$\sigma_{3i}^{s*} = 0, \qquad \sigma_{33}^{s*} = 0. \tag{28}$$

Accordingly, appropriate interfacial conditions are imposed at a later stage.

At leading order, we integrate the above equations across the thickness, neglecting $O(\eta^2)$ terms. As a result, we have

$$v_i^{s*} = V_i^s(\xi_1,\xi_2,\tau), \quad v_3^{s*} = -\frac{h\nu_s}{1-\nu_s}\zeta_s \operatorname{div}_* \mathbf{V}_{\rm tg}^s + V_3^s(\xi_1,\xi_2,\tau), \tag{29}$$

$$\sigma_{ii}^{s*} = \frac{1}{1-\nu_s^2}\left(\frac{\partial V_i^s}{\partial \xi_i} + \nu_s \frac{\partial V_j^s}{\partial \xi_j}\right), \quad \sigma_{ij}^{s*} = \frac{1}{2(1+\nu_s)}\left(\frac{\partial V_i^s}{\partial \xi_j} + \frac{\partial V_j^s}{\partial \xi_i}\right) \tag{30}$$

and

$$\begin{aligned}\sigma_{3i}^{s*} = &-\frac{h\zeta_s}{1-\nu_s}\left(\frac{1}{1+\nu_s}\Delta_* V_i^s - \frac{1}{2}\frac{\partial^2 V_i^s}{\partial \xi_j^2} + \frac{1}{2}\frac{\partial^2 V_j^2}{\partial \xi_i \xi_j}\right)\\ &+ \frac{Eh\zeta_s}{2(1+\nu_c)\rho}\frac{\partial^2 V_i^s}{\partial \tau^2} + S_{3i}^s(\xi_1,\xi_2,\tau),\end{aligned} \tag{31}$$

with $\Delta_* V_i^s = \partial^2 V_i^s/\partial \xi_1^2 + \partial^2 V_i^s/\partial \xi_2^2$ and $\operatorname{div}_* \mathbf{V}_{\rm tg}^s = \partial V_1^s/\partial \xi_1 + \partial V_2^s/\partial \xi_2$, where $\mathbf{V}_{\rm tg}^s = (V_1^s, V_2^s)$ denoting the vector of leading order tangential displacements in the skin layer. Here and below the notations in capital letters stand for 2D quantities, independent of the transverse variable ζ_q.

Then, substituting the last expression into the first boundary condition in (28), we obtain

$$S_{3i}^s = \frac{h}{1-\nu_s}\left(\frac{1}{1+\nu_s}\Delta_* V_i^s - \frac{1}{2}\frac{\partial^2 V_i^s}{\partial \xi_j^2} + \frac{1}{2}\frac{\partial^2 V_j^s}{\partial \xi_i \xi_j}\right) - \frac{Eh}{2(1+\nu_c)\rho}\frac{\partial^2 V_i^s}{\partial \tau^2}, \tag{32}$$

resulting in

$$\sigma_{3i}^{s*} = \frac{h(1-\zeta_s)}{1-\nu_s}\left(\frac{1}{1+\nu_s}\Delta_* V_i^s - \frac{1}{2}\frac{\partial^2 V_i^s}{\partial \xi_j^2} + \frac{1}{2}\frac{\partial^2 V_j^2}{\partial \xi_i \xi_j}\right) - \frac{Eh(1-\zeta_s)}{2(1+\nu_c)\rho}\frac{\partial^2 V_i^s}{\partial \tau^2}. \tag{33}$$

In a similar manner, we deduce

$$\begin{aligned}\sigma_{33}^{s*} = &-\frac{h^2(2\zeta_s - \zeta_s^2)}{2(1-\nu_s^2)}\Delta_* \operatorname{div}_* \mathbf{V}_{\rm tg}^s + \frac{Eh^2(2(1-\nu_s)\zeta_s - \zeta_s^2)}{4(1-\nu_s)(1+\nu_c)\rho}\frac{\partial^2}{\partial \tau^2}\operatorname{div}_* \mathbf{V}_{\rm tg}^s\\ &+ \frac{Eh\zeta_s}{2(1+\nu_c)\rho}\frac{\partial^2 V_3^s}{\partial \tau^2} + S_{33}^s(\xi_1,\xi_2,\tau),\end{aligned} \tag{34}$$

where the last term in the right-hand side is determined from the second boundary condition in (28). Thus,

$$\begin{aligned}\sigma_{33}^{s*} = &\frac{h^2(1-\zeta_s)}{2(1-\nu_s^2)}\left((1-\zeta_s)\Delta_* \operatorname{div}_* \mathbf{V}_{\rm tg}^s\right.\\ &\left. - \frac{E(1+\nu_s)(1-2\nu_s-\zeta_s)}{2(1+\nu_c)\rho}\frac{\partial^2}{\partial \tau^2}\operatorname{div}_* \mathbf{V}_{\rm tg}^s\right) - \frac{Eh(1-\zeta_s)}{2(1+\nu_c)\rho}\frac{\partial^2 V_3^s}{\partial \tau^2}.\end{aligned} \tag{35}$$

Next, we write down for the stresses over the core layer

$$\sigma_{ii}^c = E_c \sigma_{ii}^{c*}, \quad \sigma_{ij}^c = E_c \sigma_{ij}^{c*}, \quad \sigma_{3i}^c = E_s \eta \sigma_{3i}^{c*}, \quad \sigma_{33}^c = E_s \eta^2 \sigma_{33}^{c*}, \tag{36}$$

keeping for the displacements the same formulae as for the skin layers, i.e.,

$$v_i^c = L v_i^{c*}, \quad v_3^c = h_c v_3^{c*}. \tag{37}$$

Now, we rewrite Eqs. (1)–(6) as

$$\frac{1}{E}\frac{\partial \sigma_{3i}^{c*}}{\partial \zeta_c} + \eta^2\left(\frac{\partial \sigma_{ii}^{c*}}{\partial \xi_i} + \frac{\partial \sigma_{ij}^{c*}}{\partial \xi_j} - \frac{1}{2(1+\nu_c)}\frac{\partial^2 v_i^{c*}}{\partial \tau^2}\right) = 0, \tag{38}$$

$$\frac{\partial \sigma_{31}^{c*}}{\partial \xi_1} + \frac{\partial \sigma_{32}^{c*}}{\partial \xi_2} + \frac{\partial \sigma_{33}^{c*}}{\partial \zeta_c} - \eta^2 \frac{E}{2(1+\nu_c)}\frac{\partial^2 v_3^{c*}}{\partial \tau^2} = 0, \tag{39}$$

and

$$\sigma_{ii}^{c*} = \frac{1}{1-\nu_c^2}\left(\frac{\partial v_i^{c*}}{\partial \xi_i} + \nu_c \frac{\partial v_j^{c*}}{\partial \xi_j}\right) + \frac{\nu_c}{E(1-\nu_c)}\sigma_{33}^{c*}, \tag{40}$$

$$\sigma_{ij}^{c*} = \frac{1}{2(1+\nu_c)}\left(\frac{\partial v_i^{c*}}{\partial \xi_j} + \frac{\partial v_j^{c*}}{\partial \xi_i}\right), \tag{41}$$

$$\frac{\partial v_3^{c*}}{\partial \zeta_c} = \frac{1}{E}\sigma_{33}^{c*} - \nu_c\left(\sigma_{11}^{c*} + \sigma_{22}^{c*}\right), \tag{42}$$

$$\frac{\partial v_i^{c*}}{\partial \zeta_c} = \frac{2(1+\nu_c)}{E}\sigma_{3i}^{c*} - \eta^2 \frac{\partial v_3^{c*}}{\partial \xi_i}. \tag{43}$$

Integrating in ζ_c, we obtain at leading order

$$v_i^{c*} = \frac{2(1+\nu_c)}{E}\zeta_c S_{3i}^c, \quad v_3^{c*} = -\frac{1+\nu_c}{2E(1-\nu_c)}\zeta_c^2\left(\frac{\partial S_{31}^c}{\partial \xi_1} + \frac{S_{32}^c}{\partial \xi_2}\right) + V_3^c, \tag{44}$$

$$\sigma_{ii}^{c*} = \frac{\zeta_c}{E(1-\nu_c)}\left((2-\nu_c)\frac{\partial S_{3i}^c}{\partial \xi_i} + \nu_c \frac{S_{3j}^c}{\partial \xi_j}\right), \quad \sigma_{ij}^{c*} = \frac{\zeta_c}{E}\left(\frac{\partial S_{3i}^c}{\partial \xi_j} + \frac{S_{3j}^c}{\partial \xi_i}\right), \tag{45}$$

and

$$\sigma_{3i}^{c*} = S_{3i}^c, \quad \sigma_{33}^{c*} = -\zeta_c\left(\frac{\partial S_{31}^c}{\partial \xi_1} + \frac{\partial S_{32}^c}{\partial \xi_2}\right). \tag{46}$$

where $S_{3i}^c = S_{3i}^c(\xi_1,\xi_2,\tau)$ and $V_3^c = V_3^c(\xi_1,\xi_2,\tau)$.

The displacement continuity along the upper interface (8) can be rewritten in dimensionless form as

$$v_m^{s*}\Big|_{\zeta_s=-1} = v_m^{c*}\Big|_{\zeta_c=1}, \qquad m = 1,2,3 \tag{47}$$

giving

$$V_i^s = \frac{2(1+\nu_c)}{E}S_{3i}^c, \tag{48}$$

and

$$\left(\frac{h\nu_s}{1-\nu_s} + \frac{1}{4(1-\nu_c)}\right)\operatorname{div}_* \mathbf{V}_{\rm tg}^s + V_3^s = V_3^c. \tag{49}$$

Then, we implement the continuity of transverse shear stresses in (8), having

$$\sigma_{3i}^{s*}\Big|_{\zeta_s=-1} = \sigma_{3i}^{c*}\Big|_{\zeta_c=1}. \tag{50}$$

As a result, we arrive at, see (33), (46), and (48)

$$\frac{1}{1+\nu_s}\Delta_* \mathbf{V}_{\rm tg}^s + \frac{1}{1-\nu_s}\operatorname{grad}_* \operatorname{div}_* \mathbf{V}_{\rm tg}^s - \frac{E}{(1+\nu_c)\rho}\left(\frac{\rho}{2h} + \frac{\partial^2}{\partial \tau^2}\right)\mathbf{V}_{\rm tg}^s = 0. \tag{51}$$

Finally, we satisfy the continuity condition for the vertical normal stresses

$$\sigma_{33}^{s*}\Big|_{\zeta_s=-1} = \sigma_{33}^{c*}\Big|_{\zeta_c=1}, \tag{52}$$

deriving from (35), (46), and (48)

$$\begin{aligned}&\frac{2h}{1-\nu_s^2}\Delta_* \operatorname{div}_* \mathbf{V}_{\rm tg}^s + \frac{E}{2(1+\nu_c)h}\operatorname{div}_* \mathbf{V}_{\rm tg}^s\\ &\qquad - \frac{E}{(1+\nu_c)\rho}\frac{\partial^2}{\partial \tau^2}\left(h \operatorname{div}_* \mathbf{V}_{\rm tg}^s + V_3^s\right) = 0.\end{aligned} \tag{53}$$

The 2D Eqs. (51) and (53) govern the leading order shear approximation. The truncation error for these equations is $O(\eta^2)$. In the next section, the similar procedure will be implemented for the derivation of the bending approximation.

4. 2D bending approximation

In this section, we adapt the scaling (18) and (19), setting in the latter

$$T = \frac{L^2}{c_{2c}h_c}, \tag{54}$$

following from (12) at $q = c$. Again, we begin with the skin layer, dimensionalizing the displacement and stress components in the same

way as for a conventional plate bending analysis, see Kaplunov et al. (2022) and references therein. We get

$$v_i^s = h_c v_i^{s*}, \qquad v_3^s = L v_3^{s*} \tag{55}$$

and

$$\sigma_{ii}^s = E_s \eta \sigma_{ii}^{s*}, \sigma_{ij}^s = E_s \eta \sigma_{ij}^{s*} \sigma_{3i}^s = E_s \eta^2 \sigma_{3i}^{s*}, \sigma_{33}^s = E_s \eta^3 \sigma_{33}^{s*}. \tag{56}$$

Hence, Eqs. (1)–(6) take the form

$$\frac{\partial \sigma_{ii}^{s*}}{\partial \xi_i} + \frac{\partial \sigma_{ij}^{s*}}{\partial \xi_j} + \frac{1}{h}\frac{\partial \sigma_{3i}^{s*}}{\partial \zeta_s} - \eta^2 \frac{E}{2(1+\nu_c)\rho}\frac{\partial^2 v_i^{s*}}{\partial \tau^2} = 0, \tag{57}$$

$$\frac{\partial \sigma_{31}^{s*}}{\partial \xi_1} + \frac{\partial \sigma_{32}^{s*}}{\partial \xi_2} + \frac{1}{h}\frac{\partial \sigma_{33}^{s*}}{\partial \zeta_s} - \frac{E}{2(1+\nu_c)\rho}\frac{\partial^2 v_3^{s*}}{\partial \tau^2} = 0, \tag{58}$$

and

$$\sigma_{ii}^{s*} = \frac{1}{1-\nu_s^2}\left(\frac{\partial v_i^{s*}}{\partial \xi_i} + \nu_s \frac{\partial v_j^{s*}}{\partial \xi_j}\right) + \eta^2 \frac{\nu_s}{1-\nu_s}\sigma_{33}^{s*}, \tag{59}$$

$$\sigma_{ij}^{s*} = \frac{1}{2(1+\nu_s)}\left(\frac{\partial v_i^{s*}}{\partial \xi_j} + \frac{\partial v_j^{s*}}{\partial \xi_i}\right), \tag{60}$$

$$\frac{\partial v_3^{s*}}{\partial \zeta_s} = -\eta^2 h \nu_s (\sigma_{11}^{s*} + \sigma_{22}^{s*}) + \eta^4 h \sigma_{33}^{s*}, \tag{61}$$

$$\frac{\partial v_i^{s*}}{\partial \zeta_s} = -h\frac{\partial v_3^{s*}}{\partial \xi_i} + \eta^2 2h(1+\nu_s)\sigma_{3i}^{s*}. \tag{62}$$

Omitting intermediate calculations, we write down

$$v_i^{s*} = -h\zeta_s \frac{\partial V_3^s}{\partial \xi_i} + V_i^s, \qquad v_3^{s*} = V_3^s \tag{63}$$

$$\sigma_{ii}^{s*} = -\frac{h\zeta_s}{1-\nu_s^2}\left(\Delta_* V_3^s - (1-\nu_s)\frac{\partial^2 V_3^s}{\partial \xi_j^2}\right) + \frac{1}{1-\nu_s^2}\left(\frac{\partial V_i^s}{\partial \xi_i} + \nu_s \frac{\partial V_j^s}{\partial \xi_j}\right), \tag{64}$$

$$\sigma_{ij}^{s*} = -\frac{h\zeta_s}{1+\nu_s}\frac{\partial^2 V_3^s}{\partial \xi_i \xi_j} + \frac{1}{2(1+\nu_s)}\left(\frac{\partial V_i^s}{\partial \xi_j} + \frac{\partial V_j^s}{\partial \xi_i}\right). \tag{65}$$

$$\sigma_{3i}^{s*} = \frac{h^2(\zeta_s^2-1)}{2(1-\nu_s^2)}\Delta_* \frac{\partial V_3^s}{\partial \xi_i} - \frac{h(\zeta_s-1)}{2(1+\nu_s)}\Delta_* V_i^s - \frac{h(\zeta_s-1)}{2(1-\nu_s)}\frac{\partial}{\partial \xi_i}\operatorname{div}_* \mathbf{V}_{\mathrm{tg}}^s, \tag{66}$$

and

$$\sigma_{33}^{s*} = -\frac{h^3(\zeta_s^3 - 3\zeta_s + 2)}{6(1-\nu_s^2)}\Delta_*^2 V_3^s + \frac{h^2(\zeta_s^2 - 2\zeta_s + 1)}{2(1-\nu_s^2)}\Delta_* \operatorname{div}_* \mathbf{V}_{\mathrm{tg}}^s + \frac{Eh(\zeta_s-1)}{2(1+\nu_c)\rho}\frac{\partial^2 V_3^s}{\partial \tau^2}, \tag{67}$$

where $V_m^s = V_m^s(\xi_1, \xi_2, \tau)$, $m = 1, 2, 3$.

The asymptotic behaviour of the displacement over the core layer is similar to (55) and given by

$$v_i^c = h_c v_i^{c*}, \qquad v_3^c = L v_3^{c*}. \tag{68}$$

At the same time, the core-layer stresses due to contrast take different asymptotic orders compared to (56). For them

$$\sigma_{ii}^c = E_c \eta \sigma_{ii}^{c*}, \sigma_{ij}^c = E_c \eta \sigma_{ij}^{c*}, \sigma_{3i}^c = E_s \eta^2 \sigma_{3i}^{c*}, \sigma_{33}^c = E_s \eta^3 \sigma_{33}^{c*}. \tag{69}$$

In this case, the dimensionless governing equations become

$$\frac{\partial \sigma_{3i}^{c*}}{\partial \zeta_c} + \eta^2 E\left(\frac{\partial \sigma_{ii}^{c*}}{\partial \xi_i} + \frac{\partial \sigma_{ij}^{c*}}{\partial \xi_j}\right) - \eta^4 \frac{E}{2(1+\nu_c)}\frac{\partial^2 v_i^{c*}}{\partial \tau^2} = 0, \tag{70}$$

$$\frac{\partial \sigma_{31}^{c*}}{\partial \xi_1} + \frac{\partial \sigma_{32}^{c*}}{\partial \xi_2} + \frac{\partial \sigma_{33}^{c*}}{\partial \zeta_c} - \eta^2 \frac{E}{2(1+\nu_c)}\frac{\partial^2 v_3^{c*}}{\partial \tau^2} = 0, \tag{71}$$

together with

$$\sigma_{ii}^{c*} = \frac{1}{1-\nu_c^2}\left(\frac{\partial v_i^{c*}}{\partial \xi_i} + \nu_c \frac{\partial v_j^{c*}}{\partial \xi_j}\right) + \frac{\nu_c}{E(1-\nu_c)}\sigma_{33}^{c*}, \tag{72}$$

$$\sigma_{ij}^{c*} = \frac{1}{2(1+\nu_c)}\left(\frac{\partial v_i^{c*}}{\partial \xi_j} + \frac{\partial v_j^{c*}}{\partial \xi_i}\right), \tag{73}$$

$$\frac{\partial v_3^{c*}}{\partial \zeta_c} = \eta^2\left(\frac{1}{E}\sigma_{33}^{c*} - \nu_c(\sigma_{11}^{c*} + \sigma_{22}^{c*})\right), \tag{74}$$

$$\frac{\partial v_i^{c*}}{\partial \zeta_c} = -\frac{\partial v_3^{c*}}{\partial \xi_i} + \frac{2(1+\nu_c)}{E}\sigma_{3i}^{c*}. \tag{75}$$

The leading order approximation is

$$v_i^{c*} = -\zeta_c \frac{\partial V_3^c}{\partial \xi_i} + \frac{2(1+\nu_c)}{E}\zeta_c S_{3i}^c, \qquad v_3^{c*} = V_3^c, \tag{76}$$

$$\sigma_{ii}^{c*} = -\frac{\zeta_c}{1-\nu_c^2}\Delta_* V_3^c + \frac{\zeta_c}{1+\nu_c}\frac{\partial^2 V_3^c}{\partial \xi_j^2} + \frac{(2-\nu_c)\zeta_c}{E(1-\nu_c)}\frac{\partial S_{3i}^c}{\partial \xi_i} + \frac{\nu_c \zeta_c}{E(1-\nu_c)}\frac{\partial S_{3j}^c}{\partial \xi_j}$$

$$\sigma_{ij} = -\frac{\zeta_c}{1+\nu_c}\frac{\partial^2 V_3^c}{\partial \xi_i \partial \xi_j} + \frac{\zeta_c}{E}\left(\frac{\partial S_{3j}^c}{\partial \xi_i} + \frac{\partial S_{3i}^c}{\partial \xi_j}\right), \tag{77}$$

$$\sigma_{3i}^{c*} = S_{3i}^c, \qquad \sigma_{33}^{c*} = -\zeta_c\left(\frac{\partial S_{31}^c}{\partial \xi_1} + \frac{\partial S_{32}^c}{\partial \xi_2}\right), \tag{78}$$

where $V_3^c = V_3^c(\xi_1, \xi_2, \tau)$ and $S_{3i}^c = S_{3i}^c(\xi_1, \xi_2, \tau)$.

Next, we apply the interfacial conditions for displacements, keeping the same form as in the previous section, see (47). As a result, we deduce

$$V_i^s = -(1+h)\frac{\partial V_3^c}{\partial \xi_i} + \frac{2(1+\nu_c)}{E}S_{3i}^c, \quad V_3^s = V_3^c. \tag{79}$$

Then, we obtain from the interfacial conditions for stresses, see (50) and (52),

$$\frac{h}{1+\nu_s}\Delta_* V_i^s + \frac{h}{1-\nu_s}\frac{\partial}{\partial \xi_i}\operatorname{div}_* \mathbf{V}_{\mathrm{tg}}^s = S_{3i}^c \tag{80}$$

and

$$\frac{\partial S_{31}^c}{\partial \xi_1} + \frac{\partial S_{32}^c}{\partial \xi_2} = \frac{2h^3}{3(1-\nu_s^2)}\Delta_*^2 V_3^s + \frac{Eh}{(1+\nu_c)\rho}\frac{\partial^2 V_3^s}{\partial \tau^2} - \frac{2h^2}{1-\nu_s^2}\Delta_* \operatorname{div}_* \mathbf{V}_{\mathrm{tg}}^s. \tag{81}$$

The relations (79)–(81) readily lead to approximate 2D equations in skin-layer displacements. They can be written as

$$\frac{1}{1+\nu_s}\Delta_* \mathbf{V}_{\mathrm{tg}}^s + \frac{1}{1-\nu_s}\operatorname{grad}_* \operatorname{div}_* \mathbf{V}_{\mathrm{tg}}^s - \frac{E}{2h(1+\nu_c)} \times \left(\mathbf{V}_{\mathrm{tg}}^s + (1+h)\operatorname{grad}_* V_3^s\right) = 0. \tag{82}$$

and

$$\frac{2h^3}{3(1-\nu_s^2)}\Delta_*^2 V_3^s + \frac{Eh}{(1+\nu_c)\rho}\frac{\partial^2 V_3^s}{\partial \tau^2} - \frac{2h(1+h)}{1-\nu_s^2}\Delta_* \operatorname{div}_* \mathbf{V}_{\mathrm{tg}}^s = 0, \tag{83}$$

where $\operatorname{grad}_* = (\partial/\partial \xi_1, \partial/\partial \xi_2)$.

5. Composite equations

Eqs. (51) and (53), derived in Section 3 can be presented in a dimensional form as

$$E_s h_s\left(\frac{1}{1+\nu_s}\Delta \mathbf{u}_{\mathrm{tg}} + \frac{1}{1-\nu_s}\operatorname{grad}\operatorname{div}\mathbf{u}_{\mathrm{tg}}\right) - \frac{E_c}{2h_c(1+\nu_c)}\mathbf{u}_{\mathrm{tg}} - 2h_s\rho_s\frac{\partial^2 \mathbf{u}_{\mathrm{tg}}}{\partial t^2} = 0, \tag{84}$$

and

$$\frac{2E_s h_s^2}{1-\nu_s^2}\Delta \operatorname{div}\mathbf{u}_{\mathrm{tg}} + \frac{E_c}{2(1+\nu_c)}\operatorname{div}\mathbf{u}_{\mathrm{tg}} - 2\rho_s h_s \frac{\partial^2}{\partial t^2}\left(h_s \operatorname{div}\mathbf{u}_{\mathrm{tg}} + w\right) = 0, \tag{85}$$

where $u_i = LV_i^s$, $w = h_c V_3^s$, i.e., they are the leading order mid-plane displacements of the skin layer, in addition $\Delta = \partial^2/\partial x_1^2 + \partial^2/\partial x_2^2$, $\operatorname{div} = \partial/\partial x_1 + \partial/\partial x_2$, $\operatorname{grad} = (\partial/\partial x_1, \partial/\partial x_2)$.

Similarly, Eqs. (82) and (83) become

$$E_s h_s \left(\frac{1}{1+\nu_s} \Delta \mathbf{u}_{\mathrm{tg}} + \frac{1}{1-\nu_s} \operatorname{grad} \operatorname{div} \mathbf{u}_{\mathrm{tg}} \right) - \frac{E_c}{2h_c(1+\nu_c)} \left(\mathbf{u}_{\mathrm{tg}} + (h_c + h_s) \operatorname{grad} w \right) = 0. \tag{86}$$

and

$$\frac{2E_s h_s^3}{3(1-\nu_s^2)} \Delta^2 w + 2h_s \rho_s \frac{\partial^2 w}{\partial t^2} - \frac{2E_s h_s (h_c + h_s)}{1-\nu_s^2} \Delta \operatorname{div} \mathbf{u}_{\mathrm{tg}} = 0, \tag{87}$$

where now $u_i = h_c V_i^s$ and $w = L V_3^s$.

Let us obtain two composite equations, supporting both bending and shear motions, using the four equations above. To this end, adapt the idea originated from the concept of matched asymptotic expansions, e.g., see, Kevorkian and Cole (2013), to Eqs. (84) and (86). Accordingly, taking their sum and then subtracting the common part from the latter, we have

$$E_s h_s \left(\frac{1}{1+\nu_s} \Delta \mathbf{u}_{\mathrm{tg}} + \frac{1}{1-\nu_s} \operatorname{grad} \operatorname{div} \mathbf{u}_{\mathrm{tg}} \right) - \frac{E_c}{2h_c(1+\nu_c)} \left(\mathbf{u}_{\mathrm{tg}} + (h_c + h_s) \operatorname{grad} w \right) - 2h_s \rho_s \frac{\partial^2 \mathbf{u}_{\mathrm{tg}}}{\partial t^2} = 0. \tag{88}$$

It can be easily verified that the terms with $\operatorname{grad} w$ and that with $\partial^2 \mathbf{u}_{\mathrm{tg}}/\partial t^2$ are of order $O(\eta^2)$ for shear and bending scaling, respectively, as follows from asymptotic analysis in Sections 3 and 4. Thus, the derived composite equation has two limiting forms, given by (84) and (86).

Construction of a composite equation for (85) and (87) is more involved. First, applying the div operator to Eqs. (84) and (86), we get

$$\frac{2E_s h_s}{1-\nu_s^2} \Delta \operatorname{div} \mathbf{u}_{\mathrm{tg}} - \frac{E_c}{2h_c(1+\nu_c)} \operatorname{div} \mathbf{u}_{\mathrm{tg}} - 2h_s \rho_s \frac{\partial^2}{\partial t^2} \operatorname{div} \mathbf{u}_{\mathrm{tg}} = 0, \tag{89}$$

and

$$\frac{2E_s h_s}{1-\nu_s^2} \Delta \operatorname{div} \mathbf{u}_{\mathrm{tg}} - \frac{E_c}{2h_c(1+\nu_c)} \left(\operatorname{div} \mathbf{u}_{\mathrm{tg}} + (h_c + h_s) \Delta w \right) = 0. \tag{90}$$

As a consequence, Eqs. (85) and (87) can be rewritten as

$$2\rho_s h_s \frac{\partial^2 w}{\partial t^2} - \frac{E_c (h_s + h_c)}{2h_c(1+\nu_c)} \operatorname{div} \mathbf{u}_{\mathrm{tg}} = 0 \tag{91}$$

and

$$\frac{2E_s h_s^3}{3(1-\nu_s^2)} \Delta^2 w - \frac{E_c (h_c + h_s)^2}{2h_c(1+\nu_c)} \Delta w + 2h_s \rho_s \frac{\partial^2 w}{\partial t^2} - \frac{E_c (h_c + h_s)}{2h_c(1+\nu_c)} \operatorname{div} \mathbf{u}_{\mathrm{tg}} = 0. \tag{92}$$

Then, implementing the matching idea, we conclude that (92) is the sought for composite equation. It is clear that the terms with Δ^2 and Δ in this equation are of order $O(\eta^2)$ for shear scaling, see Section 3, i.e., the associated limiting behaviour is given by (91) as might be expected.

Thus, the derived 2D Eqs. (88) and (92) govern both bending and shear low-frequency motions of a thin high-contrast three-layered plate. It is remarkable that these equations also involve an extra scaling, which is neither a bending nor a shear one. This was not initially expected and is discovered through dispersion analysis in the next section followed by the asymptotic justification in Appendix.

6. Dispersion analysis

The initial goal of the dispersion analysis below is to validate numerically the derived 2D approximate equations by comparison with the full transcendental dispersion relations related to plane and antiplane motions.

Consider a time-harmonic wave $u_n = U_n(x_3) e^{i(kx_1 - \omega t)}$, $n = 1, 2$, $w = W(x_3) e^{i(kx_1 - \omega t)}$. First, setting $u_1 = w = 0$ and $\partial/\partial x_2 = 0$ in Eqs. (88) and (92), we obtain for the antiplane motion

$$\frac{E_s h_s}{1+\nu_s} \frac{\partial^2 u_2}{\partial x_1^2} - \frac{E_c}{2(1+\nu_c)h_c} u_2 - 2\rho_s h_s \frac{\partial^2 u_2}{\partial t^2} = 0, \tag{93}$$

resulting in the dispersion relation

$$\Omega^2 = \frac{r}{2h} + \delta \frac{(1+\nu_c)}{(1+\nu_s)} K^2, \tag{94}$$

where the dimensionless frequency and wavenumber are taken in the form

$$\Omega = \frac{\omega h_c}{c_{2c}}, \qquad K = k h_c, \tag{95}$$

with

$$c_{2c}^2 = \frac{E_c}{2(1+\nu_c)\rho_c} \quad \text{and} \quad \delta = \frac{r}{\varepsilon} = \frac{\rho_c E_s}{\rho_s E_c} \sim 1. \tag{96}$$

It can easily be verified that formula (94) is in full agreement with that previously derived in Prikazchikova et al. (2020), under the assumptions

$$\Omega \ll 1 \quad \text{and} \quad K \ll 1, \tag{97}$$

corresponding to the long-wave low-frequency approximation.

For the plane-strain case ($u_2 = 0$ and $\partial/\partial x_2 = 0$), Eqs. (88) and (92) reduce to

$$\frac{2E_s h_s^3}{3(1-\nu_s^2)} \frac{\partial^4 w}{\partial x_1^4} - \frac{E_c (h_c + h_s)^2}{2(1+\nu_c)h_c} \frac{\partial^2 w}{\partial x_1^2} + 2\rho_s h_s \frac{\partial^2 w}{\partial t^2} - \frac{E_c (h_c + h_s)}{2(1+\nu_c)h_c} \frac{\partial u_1}{\partial x_1} = 0, \tag{98}$$

and

$$\frac{2E_s h_s}{1-\nu_s^2} \frac{\partial^2 u_1}{\partial x_1^2} - \frac{E_c}{2(1+\nu_c)h_c} u_1 - 2\rho_s h_s \frac{\partial^2 u_1}{\partial t^2} - \frac{E_c (h_c + h_s)}{2(1+\nu_c)h_c} \frac{\partial w}{\partial x_1} = 0. \tag{99}$$

The associated dispersion equation can be presented as

$$\frac{E_c}{E_s} \Omega^2 - \frac{2(4h_s^2 + 6h_c h_s + 3h_c^2)(1+\nu_c)\rho_c}{3(1-\nu_s^2)h_c^2 \rho_s} K^4 + (1+\nu_c) \left(\frac{E_c (h_c + h_s)^2}{E_s (1+\nu_c) h_c^2} + \frac{4h_s}{(1-\nu_s^2)h_c} \right) K^2 \Omega^2 + \frac{4h_s^3 (1+\nu_c)}{3h_c^3 (1-\nu_s^2)} K^4 \Omega^2 - \frac{8E_s h_s^3 (1+\nu_c)^2 \rho_c}{3E_c h_c^3 (1-\nu_s^2)^2 \rho_s} K^6 - 2\frac{E_c h_s \rho_s}{E_s h_c \rho_c} \Omega^4 = 0. \tag{100}$$

It is clear that over the domain (97), the term with $K^4 \Omega^2$ can be neglected at leading order along with the term in brackets with $K^2 \Omega^2$ provided that $E_c \ll E_s$ for a high contrast. In this case, we may rewrite the last equation as

$$\varepsilon \Omega^2 + \varepsilon N_1 K^4 + N_2 K^2 \Omega^2 + N_3 K^6 + N_4 \Omega^4 = 0, \tag{101}$$

with the quantities $N_m \sim 1$, $m = 1, 2, 3, 4$, given by

$$N_1 = -\frac{2\delta(4h^2 + 6h + 3)(1+\nu_c)}{3(1-\nu_s^2)}, \qquad N_2 = \frac{4h(1+\nu_c)}{(1-\nu_s^2)}, \qquad N_3 = -\frac{8\delta h^3 (1+\nu_c)^2}{3(1-\nu_s^2)^2}, \qquad N_4 = -\frac{2h}{\delta}, \tag{102}$$

where, as before, $h = h_s/h_c$. Eq. (101) coincides with the leading order long-wave low-frequency expansion of the full dispersion relation in Kaplunov et al. (2017).

At $K = 0$, both dispersion relations (94) and (101) define the cut-off frequency

$$\Omega = \sqrt{\frac{r}{2h}}, \tag{103}$$

corresponding to the lowest shear thickness resonance of the considered three-layered plate. In addition, Eqs. (94) and (101) at $\Omega = 0$ predict the static slowly decaying components, specific for high contrast. For them

$$K = i \sqrt{\frac{\varepsilon(1+\nu_s)}{2h(1+\nu_c)}} \tag{104}$$

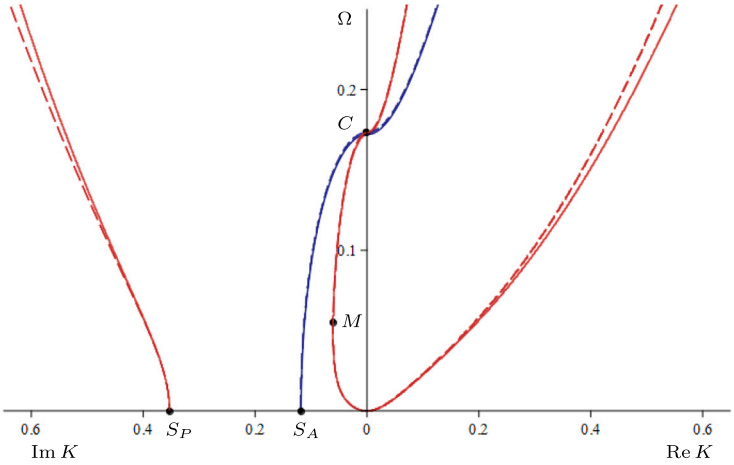

Fig. 3. Antiplane (solid blue) and plane-strain (solid red) exact dispersion curves according to Kaplunov et al. (2021, 2017) together with corresponding asymptotic relations (94) and (101), depicted with dashed blue and dashed red lines, respectively. (For interpretation of the references to colour in this figure legend, the reader is referred to the web version of this article.)

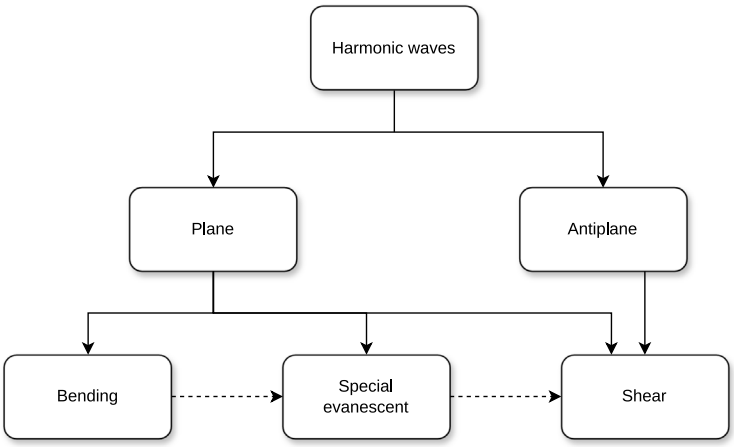

Fig. 4. Classification of harmonic waves.

and

$$K = i\sqrt{\frac{\varepsilon(1-\nu_s^2)(4h^2+6h+3)}{4h^3(1+\nu_c)}}, \tag{105}$$

respectively. These expressions are the same as those obtained in Kaplunov et al. (2021) and Erbaş et al. (2026).

The numerical illustration is presented in Fig. 3 for hypothetical parameters $E_c = 1$, $E_s = 75$, $\nu_c = 0.3$, $\nu_s = 0.365$, $\rho_c = 3$, $\rho_s = 100$, $h_c = 1$, $h_s = 1$. The dispersion curves given by Eqs. (94) and (101) are compared with their counterparts calculated from the exact transcendental dispersion relations, e.g. see Kaplunov et al. (2017, 2021). The point C in this figure stands for the cut-off frequency (103), while the points S_A and S_P correspond to estimations (104) and (105), respectively. In addition, we mark the point M, related to the vertical tangent. The figure displays both evanescent (K is imaginary) and propagating (K is real) modes. The fundamental propagating mode with zero cut-off is similar to that in the classical theory for plate bending. The plane and antiplane shear modes, having a small cut-off (103) at the point C, are typical of high contrast. Fig. 3 demonstrates a high accuracy of the tested 2D model over a broad parameter range (up to $|K| \approx 0.5$ and $\Omega \approx 0.2$) for all low-frequency modes specific of a studied high-contrast laminate. In addition, we remark that the layout chosen for this figure (see also the diagram in Fig. 4) involving plane and antiplane as well as propagating and evanescent waves appears to be optimal for visualizing the results of numerical comparison.

It is worth noting that the points S_A and C belong to the same curve, implying that the antiplane shear propagating mode originates from the associated static limit. However, it is not the case for the plane shear propagating mode, having the same cut-off at the point C, which is not connected with the point S_P corresponding to statics. In contrast to the antiplane scenario, the plane evanescent mode approaching the cut-off at the point C starts from the origin. At the same time, near the origin this mode supports the so-called dynamic edge effect in the classical plate bending theory, see Bolotin (1961). Thus, the curve connecting the origin and the point C follows bending regime near the origin and shear one in the vicinity of the point C. Consequently, we may expect a transition region between these two regimes somewhere around the point M in Fig. 3.

Let us complement the presented phenomenological observations with a more rigorous asymptotic reasoning. To this end, we study the dispersion relation (101) over the finer frequency and wavenumber subdomains within the range given by (97).

First, we deduce that at $\boldsymbol{\Omega} \ll \boldsymbol{\varepsilon}$ the quasi-static limit (105), for which $K \sim \varepsilon^{1/2}$, holds along with the shortened dispersion relation

$$\Omega^2 + N_1 K^4 = 0, \tag{106}$$

valid for $K \ll \varepsilon^{1/2}$. It supports one propagating and one evanescent mode, according to the classical theory for plate bending.

At $\boldsymbol{\Omega} \sim \boldsymbol{\varepsilon}$, we have from (101) at the leading order

$$\varepsilon\Omega^2 + \varepsilon N_1 K^4 + N_2 K^2 \Omega^2 + N_3 K^6 = 0, \tag{107}$$

dictating that $K \sim \varepsilon^{1/2}$. This bi-cubic equation governs two evanescent and one propagating mode as can be easily verified by looking at the sign of N_3.

Over the interval $\boldsymbol{\varepsilon \ll \Omega \ll \varepsilon^{3/4}}$ we observe the degeneration in (101) at

$$K^2 \approx -\frac{\varepsilon}{N_2}. \tag{108}$$

In this case, we obtain in (101), $\varepsilon N_1 K^4 \sim N_3 K^6 \sim \varepsilon^3$, whereas $N_4 \Omega^4 \ll \varepsilon^3$ resulting in

$$K^2 = -\frac{\varepsilon}{N_2} + \frac{(N_3 - N_1 N_2)}{N_2^4}\frac{\varepsilon^3}{\Omega^2} \tag{109}$$

with $K \sim \varepsilon^{1/2}$.

Over this frequency interval, we also have

$$N_2 \Omega^2 + N_3 K^4 = 0, \tag{110}$$

which in fact holds true over a broader range, namely at $\varepsilon \ll \Omega \ll 1$ with $K^2 \sim \Omega$.

At $\boldsymbol{\Omega \sim \varepsilon^{3/4}}$, we have to keep all terms in (101), getting

$$K^2 = -\frac{\varepsilon}{N_2} + \frac{(N_3 - N_1 N_2)}{N_2^4}\frac{\varepsilon^3}{\Omega^2} - \frac{N_4}{N_2}\Omega^2, \tag{111}$$

with $K \sim \varepsilon^{1/2}$ as above. The derivative of the last expression with respect to Ω equals to zero when

$$\Omega = \varepsilon^{3/4} \sqrt[4]{\frac{(N_1 N_2 - N_3)}{N_2^3 N_4}}, \tag{112}$$

corresponding to the point M in Fig. 3. It can be verified, see Appendix, that at this point the studied evanescent mode is governed by the second-order Eq. (A.45), balancing the extension of the skin layer and Winkler-type response of the core layer.

Finally, over the region $\boldsymbol{\varepsilon^{3/4} \ll \Omega \ll 1}$, Eq. (101) becomes

$$K^2 = -\frac{\varepsilon}{N_2} - \frac{N_4}{N_2}\Omega^2 \tag{113}$$

with $K \sim \varepsilon^{1/2}$ if $\Omega \lesssim \varepsilon^{1/2}$ and $K \sim \Omega$ when $\Omega \gg \varepsilon^{1/2}$, except the narrow vicinity of the cut-off frequency where $K \ll \varepsilon^{1/2}$.

The developed asymptotic analysis provides a better understanding of the peculiarities of the dispersion curve connecting the origin and the point C. In particular, formulae (106) and (107) indicate that for $0 \le \Omega \lesssim \varepsilon$, $K^2 \sim \Omega$ and therefore are in line with the asymptotic scaling for bending, adopted in Section 4. At the same time, formula (113) demonstrates that, generally, $K \sim \Omega$ for $\varepsilon^{1/2} \lesssim \Omega \ll 1$ is in agreement with the scaling supporting shear, see Section 3.

Thus, the transition from bending to shear type asymptotic behaviour for the considered plane evanescent mode occurs over the interval $\varepsilon \ll \Omega \lesssim \varepsilon^{3/4}$, see formulae (109), (111) as well as the estimation for the point M, given by (112). It is obvious that along this interval the asymptotic scaling does not coincide with neither bending nor shear one. In particular, when $\Omega \sim \varepsilon^{3/4}$, we have $K \sim \varepsilon^{1/2}$, hence, $\Omega \sim K^{3/2}$. This additional scaling is not part of the derivation in the main body of the paper. However, as shown in the Appendix, the established two-dimensional Eqs. (88) and (92) involve a special shortened form, originated from the discovered new scaling.

Fig. 5 illustrates the transition from the bending to shear mode localized near zero and the lowest cutoff frequencies, respectively, see (106) and (113), along with (111) standing for an intermediate regime. It is worth noting that each of these three formulae governs a local asymptotic behaviour, whereas uniform one is given by the five-term polynomial (101). Nevertheless, this figure shows that each of the local approximations is robust as expected.

It is also interesting that the dispersion curve for the evanescent mode originated at the point S_P is governed by the quasi-static limit, see formula (105) at $\Omega \ll \varepsilon$ and the expressions (107) and (110) for $\varepsilon \lesssim \Omega \ll 1$. Further details on the dispersion of elastic waves in a high-contrast three-layered plate can be found in Kaplunov et al. (2017), Prikazchikova et al. (2024) and Kaplunov et al. (2021).

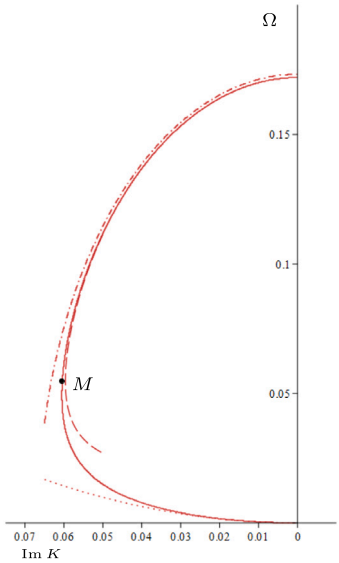

Fig. 5. Dispersion curves for evanescent plane wave according to exact transcendental dispersion relation in Kaplunov et al. (2017) (solid line), together with shortened relations corresponding to bending (106) (dotted line), shear (113) (dash–dot line), and the transitional regime (111) around point M (dashed line).

7. Conclusions

The derived 2D three-mode approximation governs a bending wave along with plane and antiplane shear waves with a low-frequency cut-off. It accommodates three asymptotic scalings. Two of them referred to in the paper as bending and shear ones, have a lot of in common with those characteristic of homogeneous plates. Contrary, the third scaling is typical for the considered sandwich plate only. It governs the transition from bending to shear behaviour for one of the plane evanescent waves and was spotted only when plotting dispersion curves.

Thus, the results of multiparametric dispersion analysis covering both plane and antiplane waves and not restricted to propagating ones only appears to be an important part of the asymptotic consideration. Comparison of the shortened polynomial dispersion relations with the exact transcendental equations enables numerical validation of the former. In this case, the excellent accuracy of the polynomial predictions exceeds the initial expectations arising from the formal $O(\eta^2)$ relative truncation error of the established approximate model.

Another valuable contribution is concerned with the merging of the 2D approximations corresponding to bending and shear scalings. It extends to differential equations the idea of matched expansions oriented to asymptotic series in terms of a small or large parameter.

The dynamic equations derived in the paper can be subject to boundary conditions as well as incorporate the effect of appropriate surface loads similar to their static counterparts, see Erbaş et al. (2026). In this case, the associated boundary-value problems may admit analytical solutions for canonical (rectangular and circular) domains.

The constraints imposed in the paper may be relaxed, including the assumption of no significant contrast in layers' thicknesses, e.g., the scenario of thin skins is of obvious interest for modelling of a variety of sandwich structures. In the latter case, however, one should expect a different asymptotic theory generalizing the approach established in the paper. This is also true for other parametric setups, e.g. those not following the key assumption $\varepsilon \sim r$ on the relation between the contrast parameters in the formula (9), see Kaplunov et al. (2017) and Prikazchikova et al. (2020) for further detail. The developed methodology has a potential to be implemented for numerous challenging problems concerned with high contrast laminates, including but not

restricted to the modelling of symmetric deformation of the sandwich studied here, as well as analysis of multilayered asymmetric structures. Another important extension is concerned with analysis of anisotropic laminates taking into account non-perfect bonding of the layers.

CRediT authorship contribution statement

Barış Erbaş: Writing – review & editing, Writing – original draft, Visualization, Validation, Methodology, Investigation, Formal analysis, Conceptualization. **Ludmila Prikazchikova:** Writing – review & editing, Writing – original draft, Visualization, Validation, Supervision, Methodology, Investigation, Formal analysis, Conceptualization. **Julius Kaplunov:** Writing – review & editing, Writing – original draft, Visualization, Validation, Supervision, Methodology, Investigation, Formal analysis, Conceptualization.

Declaration of competing interest

The authors declare that they have no known competing financial interests or personal relationships that could have appeared to influence the work reported in this paper.

Acknowledgements

The authors gratefully acknowledge support from the Engineering and Physical Sciences Research Council (EPSRC) [EP/Y021983/1].

Appendix. Special scaling

For simplicity, consider time-harmonic, plane-strain motion setting for the vibration frequency

$$\frac{\omega h_c}{c_{2c}} = \varepsilon^{3/4}\Omega_* = \eta^{3/2}E^{3/4}\Omega_* \tag{A.1}$$

with $\Omega_* \sim 1$. This frequency band corresponds to the vicinity of the point M in Fig. 3, where the shortened dispersion relation is given by (111). Therefore, now,

$$T \sim \frac{L^{3/2}}{h_q^{1/2}c_q}, \tag{A.2}$$

in contrast to shear and bending scalings given by (12) and (13), respectively. In this case, the displacements have to be taken of the same order, i.e.,

$$v_1^q = Lv_1^{q*}, \qquad v_3^q = Lv_3^{q*}. \tag{A.3}$$

Then, nondimensional stresses for skin layers can be defined as

$$\sigma_{ii}^s = E_s\sigma_{ii}^{s*}, \qquad \sigma_{31}^s = E_s\eta\sigma_{31}^{s*}, \qquad \sigma_{33}^s = E_s\eta^2\sigma_{33}^{s*}. \tag{A.4}$$

As a result, the plane-strain form of Eqs. (1)–(6) at $q = s$ becomes

$$\frac{\partial\sigma_{11}^{s*}}{\partial\xi_1} + \frac{1}{h}\frac{\partial\sigma_{31}^{s*}}{\partial\zeta_s} + \eta\frac{E^{5/2}}{2(1+\nu_c)\rho}\Omega_*^2 v_1^{s*} = 0, \tag{A.5}$$

$$\frac{\partial\sigma_{31}^{s*}}{\partial\xi_1} + \frac{1}{h}\frac{\partial\sigma_{33}^{s*}}{\partial\zeta_s} + \frac{E^{5/2}}{2(1+\nu_c)\rho}\Omega_*^2 v_3^{s*} = 0, \tag{A.6}$$

and

$$\sigma_{11}^{s*} = \frac{1}{1-\nu_s^2}\frac{\partial v_1^{s*}}{\partial\xi_1} + \eta^2\frac{\nu_s}{1-\nu_s}\sigma_{33}^{s*}, \tag{A.7}$$

$$\sigma_{22}^{s*} = \frac{\nu_s}{1-\nu_s^2}\frac{\partial v_1^{s*}}{\partial\xi_1} + \eta^2\frac{\nu_s}{1-\nu_s}\sigma_{33}^{s*}, \tag{A.8}$$

$$\frac{\partial v_3^{s*}}{\partial\zeta_s} = -\eta h\left(\nu_s(\sigma_{11}^{s*} + \sigma_{22}^{s*}) - \eta^2\sigma_{33}^{s*}\right), \tag{A.9}$$

$$\frac{\partial v_1^{s*}}{\partial\zeta_s} = -\eta h\left(\frac{\partial v_3^{s*}}{\partial\xi_1} - 2\eta(1+\nu_s)\sigma_{31}^{s*}\right). \tag{A.10}$$

In contrast to the considerations in the main body of the paper, we cannot restrict ourselves to leading order expansions due to the degeneration observed through dispersion analysis in Section 6. Now, we have to set

$$v_n^q = v_n^{q,0} + \eta\, v_n^{q,1} + \cdots, \qquad n = 1, 3 \tag{A.11}$$

for displacements ($q = s$) and similarly for stresses.

At leading order, we get

$$v_1^{s,0} = V_1^{s,0}(\xi_1), \qquad v_3^{s,0} = V_3^{s,0}(\xi_1) \tag{A.12}$$

and

$$\sigma_{11}^{s,0} = \frac{1}{1-\nu_s^2}\frac{dV_1^{s,0}}{d\xi_1}, \qquad \sigma_{22}^{s,0} = \frac{\nu_s}{1-\nu_s^2}\frac{dV_1^{s,0}}{d\xi_1}, \tag{A.13}$$

$$\sigma_{31}^{s,0} = \frac{h(1-\zeta_s)}{1-\nu_s^2}\frac{d^2V_1^{s,0}}{d\xi_1^2}, \tag{A.14}$$

$$\sigma_{33}^{s,0} = \frac{h(1-\zeta_s)}{2}\left(\frac{h(1-\zeta_s)}{1-\nu_s^2}\frac{d^3V_1^{s,0}}{d\xi_1^3} + \frac{E^{5/2}}{2(1+\nu_c)\rho}\Omega_*^2 V_3^{s,0}\right).$$

Then, the next order corrections become

$$v_1^{s,1} = -h\zeta_s\frac{dV_3^{s,0}}{d\xi_1} + V_1^{s,1}(\xi_1), \qquad v_3^{s,1} = -\frac{h\nu_s}{1-\nu_s}\zeta_s\frac{dV_1^{s,0}}{d\xi_1}, \tag{A.15}$$

and

$$\sigma_{11}^{s,1} = -\frac{h\zeta_s}{1-\nu_s^2}\frac{d^2V_3^{s,0}}{d\xi_1^2} + \frac{1}{1-\nu_s^2}\frac{dV_1^{s,1}}{d\xi_1}, \tag{A.16}$$

$$\sigma_{22}^{s,1} = -\frac{h\nu_s\zeta_s}{1-\nu_s^2}\frac{d^2V_3^{s,0}}{d\xi_1^2} + \frac{\nu_s}{1-\nu_s^2}\frac{dV_1^{s,1}}{d\xi_1}, \tag{A.17}$$

$$\sigma_{31}^{s,1} = \frac{h(\zeta_s-1)}{1-\nu_s^2}\left(\frac{h(\zeta_s+1)}{2}\frac{d^3V_3^{s,0}}{d\xi_1^3} - \frac{d^2V_1^{s,1}}{d\xi_1^2} - \frac{E^{5/2}(1-\nu_s^2)}{2(1+\nu_c)\rho}\Omega_*^2 V_1^{s,0}\right), \tag{A.18}$$

$$\sigma_{33}^{s,1} = -\frac{h^2(\zeta_s-1)^2}{2(1-\nu_s^2)}\left(\frac{h(\zeta_s+2)}{3}\frac{d^4V_3^{s,0}}{d\xi_1^4} + \frac{d^3V_1^{s,1}}{d\xi_1^3}\right) + \frac{E^{5/2}h^2}{4(1-\nu_s)(1+\nu_c)\rho}(\zeta_s^2 - 2(1-\nu_s)\zeta_s + 1 - 2\nu_s)\Omega_*^2\frac{dV_1^{s,0}}{d\xi_1}. \tag{A.19}$$

For the core layer, we nondimensionalize stresses as

$$\sigma_{ii} = E_c\sigma_{ii}^{c*}, \quad \sigma_{31} = \eta E_s\sigma_{31}^{c*}, \quad \sigma_{33} = \eta^2 E_s\sigma_{ii}^{c*}. \tag{A.20}$$

keeping for the dimensionless displacements the former formula (A.3) taken at $q = c$. Next, we obtain from Eqs. (1)–(6)

$$E\eta^2\frac{\partial\sigma_{11}^{s*}}{\partial\xi_1} + \frac{\partial\sigma_{31}^{s*}}{\partial\zeta_c} + \eta^3\frac{E^{5/2}}{2(1+\nu_c)}\Omega_*^2 v_1^{c*} = 0, \tag{A.21}$$

$$\frac{\partial\sigma_{31}^{s*}}{\partial\xi_1} + \frac{\partial\sigma_{33}^{s*}}{\partial\zeta_c} + \eta^2\frac{E^{5/2}}{2(1+\nu_c)}\Omega_*^2 v_3^{c*} = 0, \tag{A.22}$$

and

$$\sigma_{11}^{c*} = \frac{1}{1-\nu_c^2}\frac{\partial v_1^{c*}}{\partial\xi_1} + \frac{\nu_c}{E(1-\nu_c)}\sigma_{33}^{c*}, \tag{A.23}$$

$$\sigma_{22}^{s*} = \frac{\nu_c}{1-\nu_c^2}\frac{\partial v_1^{c*}}{\partial\xi_1} + \frac{\nu_c}{E(1-\nu_c)}\sigma_{33}^{c*}, \tag{A.24}$$

$$\frac{\partial v_3^{c*}}{\partial\zeta_c} = \eta\left(\frac{1}{E}\sigma_{33}^{s*} - \nu_c(\sigma_{11}^{c*} + \sigma_{22}^{c*})\right), \tag{A.25}$$

$$\frac{\partial v_1^{c*}}{\partial\zeta_c} = -\eta\frac{\partial v_3^{c*}}{\partial\xi_1} + \frac{2(1+\nu_c)}{E}\sigma_{31}^{c*}. \tag{A.26}$$

Then, the coefficients in the sought for two-term expansions, see (A.11), take the form

$$v_3^{c,0} = V_3^{c,0}(\xi_1), \quad v_1^{c,0} = \frac{2(1+\nu_c)\zeta_c}{E}S_{31}^{c,0}(\xi_1), \tag{A.27}$$

$$\sigma_{31}^{c,0} = S_{31}^{c,0}(\xi_1), \quad \sigma_{33}^{c,0} = -\zeta_c \frac{dS_{31}^{c,0}}{d\xi_1}, \tag{A.28}$$

$$\sigma_{11}^{c,0} = \frac{(2-\nu_c)\zeta_c}{E(1-\nu_c)} \frac{dS_{31}^{c,0}}{d\xi_1}, \quad \sigma_{22}^{c,0} = \frac{\nu_c \zeta_c}{E(1-\nu_c)} \frac{dS_{31}^{c,0}}{d\xi_1}, \tag{A.29}$$

and

$$v_1^{c,1} = -\zeta_c \frac{dV_3^{c,0}}{d\xi_1} + \frac{2(1+\nu_c)\zeta_c}{E} S_{31}^{c,1}(\xi_1),$$
$$v_3^{c,1} = -\frac{(1+\nu_c)\zeta_c^2}{2E(1-\nu_c)} \frac{dS_{31}^{c,0}}{d\xi_1} + V_3^{c,1}(\xi_1), \tag{A.30}$$

$$\sigma_{31}^{c,1} = S_{31}^{c,1}(\xi_1), \quad \sigma_{33}^{c,1} = -\zeta_c \frac{dS_{31}^{c,1}}{d\xi_1}. \tag{A.31}$$

Now, consider the continuity conditions along the interface. At leading order, they take the form

$$V_1^{s,0} = \frac{2(1+\nu_c)}{E} S_{31}^{c,0}, \quad V_3^{s,0} = V_3^{c,0}, \tag{A.32}$$

$$\frac{2h}{1-\nu_s^2} \frac{d^2 V_1^{s,0}}{d\xi_1^2} = S_{31}^{c,0}, \tag{A.33}$$

and

$$\frac{2h^2}{1-\nu_s^2} \frac{d^3 V_1^{s,0}}{d\xi_1^3} + \frac{E^{5/2}h}{(1+\nu_c)\rho} \Omega_*^2 V_3^{s,0} = -\frac{dS_{31}^{c,0}}{d\xi_1}. \tag{A.34}$$

Next, we derive from these formulae two ordinary differential equations given by

$$\frac{2h}{1-\nu_s^2} \frac{d^2 V_1^{s,0}}{d\xi_1^2} - \frac{E}{2(1+\nu_c)} V_1^{s,0} = 0 \tag{A.35}$$

and

$$\frac{2h(1+h)}{1-\nu_s^2} \frac{d^3 V_1^{s,0}}{d\xi_1^3} + \frac{E^{5/2}h}{(1+\nu_c)\rho} \Omega_*^2 V_3^{s,0} = 0. \tag{A.36}$$

At next order, the continuity conditions are written as

$$h \frac{dV_3^{s,0}}{d\xi_1} + V_1^{s,1} = -\frac{dV_3^{c,0}}{d\xi_1} + \frac{2(1+\nu_c)}{E} S_{31}^{c,1}, \tag{A.37}$$

$$\frac{h\nu_s}{1-\nu_s} \frac{dV_1^{s,0}}{d\xi_1} = -\frac{1+\nu_c}{2E(1-\nu_c)} \frac{dS_{31}^{c,0}}{d\xi_1} + V_3^{c,1}, \tag{A.38}$$

$$\frac{2h}{1-\nu_s^2} \frac{d^2 V_1^{s,1}}{d\xi_1^2} + \frac{E^{5/2}h}{(1+\nu_c)\rho} \Omega_*^2 V_1^{s,0} = S_{31}^{c,1}, \tag{A.39}$$

and

$$\frac{2h^3}{3(1-\nu_s^2)} \frac{d^4 V_3^{s,0}}{d\xi_1^4} - \frac{2h^2}{1-\nu_s^2} \frac{d^3 V_1^{s,1}}{d\xi_1^3} - \frac{E^{5/2}h^2}{(1+\nu_c)\rho} \Omega_*^2 \frac{dV_1^{s,0}}{d\xi_1} = \frac{dS_{31}^{c,1}}{d\xi_1}. \tag{A.40}$$

As before, we also have

$$\frac{2h}{1-\nu_s^2} \frac{d^2 V_1^{s,1}}{d\xi_1^2} - \frac{E}{2(1+\nu_c)} V_1^{s,1} + \frac{E^{5/2}h}{(1+\nu_c)\rho} \Omega_*^2 V_1^{s,0} = \frac{E(1+h)}{2(1+\nu_c)} \frac{dV_3^{s,0}}{d\xi_1}, \tag{A.41}$$

and

$$\frac{2h^3}{3(1-\nu_s^2)} \frac{d^4 V_3^{s,0}}{d\xi_1^4} - \frac{2h(1+h)}{1-\nu_s^2} \frac{d^3 V_1^{s,1}}{d\xi_1^3} - \frac{E^{5/2}h(1+h)}{(1+\nu_c)\rho} \Omega_*^2 \frac{dV_1^{s,0}}{d\xi_1} = 0. \tag{A.42}$$

Finally, we add (A.35) and (A.41), taking into account (A.36). Denoting $V_1^s = V_1^{s,0} + \eta V_1^{s,1}$, we arrive, to within $O(\eta^2)$ truncation error, at

$$\frac{2h}{1-\nu_s^2} \frac{d^2 V_1^s}{d\xi_1^2} - \frac{E}{2(1+\nu_c)} V_1^s + \eta \left(\frac{E^{5/2}h}{(1+\nu_c)\rho} \Omega_*^2 V_1^s + \frac{(1+h)^2 \rho}{4hE^{1/2}(1+\nu_c)\Omega_*^2} \frac{d^2 V_1^s}{d\xi_1^2} \right) = 0. \tag{A.43}$$

In dimensional variables, the last equation takes the form

$$\left(\frac{2E_s h_s}{1-\nu_s^2} + \frac{(h_c+h_s)^2 E_c^2}{8h_c^2 h_s (1+\nu_c)^2 \rho_s \omega^2} \right) \frac{d^2 u_1}{dx_1^2} + \left(2h_s \rho_s \omega^2 - \frac{E_c}{2h_c(1+\nu_c)} \right) u_1 = 0, \tag{A.44}$$

where $u_1 = LV_1^s$. It can easily be verified that the shortened dispersion relation (111) follows from this equation. Also, at the vibration frequency given by (112), (A.44) may be reduced to

$$\frac{2E_s h_s}{1-\nu_s^2} \frac{d^2 u_1}{dx_1^2} - \frac{E_c}{2h_c(1+\nu_c)} u_1 = 0, \tag{A.45}$$

being the dimensional counterpart of (A.35). It is satisfied at the wave number given by (108).

Our next goal is to demonstrate that the time-harmonic limiting behaviour of the composite formulation (98) and (99), under the special scaling defined in this Appendix, leads to Eq. (A.44). Using relation (A.1), and setting $u_n = LV_n^s$, $n = 1, 3$, according to (A.3), we deduce from (98) and (99), respectively

$$\frac{2h^2}{1-\nu_s^2} \frac{d^3 V_1^s}{d\xi_1^3} + \frac{E}{2(1+\nu_c)} \frac{dV_1^s}{d\xi_1} + \frac{E^{5/2}h}{(1+\nu_c)\rho} \Omega_*^2 V_3^s - \eta \left(\frac{2h^3}{3(1-\nu_s^2)} \frac{d^4 V_3^s}{d\xi_1^4} - \frac{E(1+h)}{2(1+\nu_c)} \frac{d^2 V_3^s}{d\xi_1^2} - \frac{E^{5/2}h^2}{(1+\nu_c)\rho} \Omega_*^2 \frac{dV_1^s}{d\xi_1} \right) = 0, \tag{A.46}$$

and

$$\frac{2h}{1-\nu_s^2} \frac{d^2 V_1^s}{d\xi_1^2} - \frac{E}{2(1+\nu_c)} V_1^s - \eta \left(\frac{E(1+h)}{2(1+\nu_c)} \frac{dV_3^s}{d\xi_1} - \frac{E^{5/2}h}{(1+\nu_c)\rho} \Omega_*^2 V_1^s \right) = 0. \tag{A.47}$$

Now, substituting the leading order part of (A.46) into (A.47), we arrive at Eq. (A.43). Thus, the special scaling in question here is also embedded into the established composite model, originally based on shear and bending scalings only.

Data availability

No data was used for the research described in the article.

References

Achenbach, J., 2012. Wave Propagation in Elastic Solids. Elsevier.

Aghalovyan, L.A., 2015. Asymptotic Theory of Anisotropic Plates and Shells. World Scientific.

Aguiar, A., Rehm, L., Steigmann, D., Taylor, M., 2025. An asymptotic thin-plate theory derived from state-based peridynamics. J. Peridyn. Nonlocal Model. 7 (1), 2.

Ashby, M.F., Gibson, L.J., 1997. Cellular Solids: Structure and Properties. Press Syndicate of the University of Cambridge, Cambridge, UK, pp. 175–231.

Aßmus, M., Bergmann, S., Naumenko, K., Altenbach, H., 2017. Mechanical behaviour of photovoltaic composite structures: A parameter study on the influence of geometric dimensions and material properties under static loading. Compos. Commun. 5, 23–26.

Baxter, S.C., Horgan, C.O., 1995. End effects for anti-plane shear deformations of sandwich structures. J. Elasticity 40 (2), 123–164.

Berdichevsky, V.L., 2009. Variational Principles of Continuum Mechanics: II. Applications. Springer Science & Business Media.

Berdichevsky, V.L., 2010. An asymptotic theory of sandwich plates. Internat. J. Engrg. Sci. 48 (3), 383–404.

Birman, V., Kardomateas, G.A., 2018. Review of current trends in research and applications of sandwich structures. Compos. B-Eng. 142, 221–240.

Bolotin, V.V., 1961. Dynamic edge effect in the elastic vibrations of plates. Inzhenernyi Sb. Eng. J. 31, 3–14.

Boutin, C., Viverge, K., 2016. Generalized plate model for highly contrasted laminates. Eur. J. Mech. A-Solids 55, 149–166.

Boutin, C., Viverge, K., Hans, S., 2021. Dynamics of contrasted stratified elastic and viscoelastic plates-application to laminated glass. Compos. B-Eng. 212, 108551.

Castanie, B., Bouvet, C., Ginot, M., 2020. Review of composite sandwich structure in aeronautic applications. Compos. C-Open 1, 100004.

Chapman, C.J., 2013. An asymptotic decoupling method for waves in layered media. Proc. R. Soc. A-Math. Phy. 469 (2153), 20120659.
Erbaş, B., Prikazchikova, L., Kaplunov, J., 2026. Asymptotic analysis of three-dimensional boundary-value problems for three-layered high-contrast plates. Proc. R. Soc. A-Math. Phy. 482 (2331).
Friedrichs, K.O., Dressler, R.F., 1961. A boundary-layer theory for elastic plates. Comm. Pure Appl. Math. 14 (1), 1–33.
Garrido, M., Madeira, J.F.A., Proença, M., Correia, J.R., 2019. Multi-objective optimization of pultruded composite sandwich panels for building floor rehabilitation. Constr. Build. Mater. 198, 465–478.
Goldenveizer, A.L., 1962. Derivation of an approximate theory of bending of a plate by the method of asymptotic integration of the equations of the theory of elasticity. J. Appl. Math. Mech.-Uss 26 (4), 1000–1025.
Goldenveizer, A.L., 1966. The principles of reducing three-dimensional problems of elasticity to two-dimensional problems of the theory of plates and shells. In: Applied Mechanics: Proceedings of the Eleventh International Congress of Applied Mechanics Munich (Germany) 1964. Springer, pp. 306–311.
Goldenveizer, A.L., 1976. Theory of Thin Elastic Shells. Izdatel'stvo Nauka.
Goldenveizer, A.L., Kaplunov, J.D., Nolde, E.V., 1993. On Timoshenko-Reissner type theories of plates and shells. Int. J. Solids Struct. 30 (5), 675–694.
Green, A.E., 1962. On the linear theory of thin elastic shells. Proc. R. Soc. A 266 (1325), 143–160.
Gregory, R.D., Wan, F.Y.M., 1984. Decaying states of plane strain in a semi-infinite strip and boundary conditions for plate theory. J. Elasticity 14 (1), 27–64.
Gregory, R.D., Wan, F.Y.M., 1985. On plate theories and Saint-Venant's principle. Int. J. Solids Struct. 21 (10), 1005–1024.
He, Z.C., Xiao, X., Li, E., 2017. Design for structural vibration suppression in laminate acoustic metamaterials. Compos. B-Eng. 131, 237–252.
Hohe, J., 2015. Load and frequency interaction effects in dynamic buckling of soft core sandwich structures. Compos. Struct. 132, 1006–1018.
Horgan, C.O., 1998. Saint-Venant end effects for sandwich structures. In: Fourth International Conference on Sanwich Construction. vol. 1, EMAS Publishing UK London, UK, pp. 191–200.
Kaplunov, J., Erbaş, B., Ege, N., 2022. Asymptotic derivation of 2D dynamic equations of motion for transversely inhomogeneous elastic plates. Internat. J. Engrg. Sci. 178, 103723.
Kaplunov, J.D., Kossovich, L.Y., Nolde, E.V., 1998. Dynamics of Thin Walled Elastic Bodies. Academic Press.
Kaplunov, J.D., Kossovich, L.Y., Rogerson, G.A., 2000. Direct asymptotic integration of the equations of transversely isotropic elasticity for a plate near cut-off frequencies. Q. J. Mech. Appl. Math. 53 (2), 323–341.
Kaplunov, J., Nolde, E., Rogerson, G.A., 2006. An asymptotic analysis of initial-value problems for thin elastic plates. Proc. R. Soc. A-Math. Phy. 462 (2073), 2541–2561.
Kaplunov, J., Prikazchikov, D.A., Prikazchikova, L.A., 2017. Dispersion of elastic waves in a strongly inhomogeneous three-layered plate. Int. J. Solids Struct. 113, 169–179.
Kaplunov, J., Prikazchikova, L., Alkinidri, M., 2021. Antiplane shear of an asymmetric sandwich plate. Contin. Mech. Therm. 33, 1247–1262.
Kevorkian, J., Cole, J.D., 2013. Perturbation Methods in Applied Mathematics. Springer Science & Business Media.
Kõrgesaar, M., Goncalves, B.R., Romanoff, J., Remes, H., 2016. Non-linear effective properties for web-core steel sandwich panels in tension. Int. J. Mech. Sci. 115, 428–437.
Le, K.C., 1997. High frequency vibrations and wave propagation in elastic shells: Variational-asymptotic approach. Int. J. Solids Struct. 34 (30), 3923–3939.
Le, K.C., 2012. Vibrations of Shells and Rods. Springer Science & Business Media.
Le, K.C., 2023. An asymptotically exact first-order shear deformation theory for functionally graded plates. Internat. J. Engrg. Sci. 190, 103875.
Lee, J., Kang, S., Ha, Y., Hong, S., 2018. Structural behavior of durable composite sandwich panels with high performance expanded polystyrene concrete. Int. J. Concr. Struct. Mater. 12 (1), 21.
Liu, K., Zong, S., Li, Y., Wang, Z., Hu, Z., Wang, Z., 2022. Structural response of the U-type corrugated core sandwich panel used in ship structures under the lateral quasi-static compression load. Mar. Struct. 84, 103198.
López-Aenlle, M., Pelayo, F., 2014. Dynamic effective thickness in laminated-glass beams and plates. Compos. B-Eng. 67, 332–347.
Martin, T.P., Layman, C.N., Moore, K.M., Orris, G.J., 2012. Elastic shells with high-contrast material properties as acoustic metamaterial components. Phys. Rev. B 85 (16), 161103.
Pichugin, A.V., Rogerson, G.A., 2001. A two-dimensional model for extensional motion of a pre-stressed incompressible elastic layer near cut-off frequencies. IMA J. Appl. Math. 66 (4), 357–385.
Prikazchikova, L., Aydın, Y.E., Erbaş, B., Kaplunov, J., 2020. Asymptotic analysis of an anti-plane dynamic problem for a three-layered strongly inhomogeneous laminate. Math. Mech. Solids 25 (1), 3–16.
Prikazchikova, L., Rege, A., Kaplunov, J., Prikazchikov, D., 2024. Low-frequency propagating and evanescent waves in strongly inhomogeneous sandwich plates. Z. Angew. Math. Phys. 75 (6), 211.
Qiu, Y., Yan, R., Shen, W., Li, X., Ye, Z., Li, J., Xu, Z., 2023. Load-bearing characteristics of marine complex sandwich composites considering unequal elastic modulus in tension and compression. Mar. Struct. 89, 103382.
Rogacheva, N.N., 2020. The Theory of Piezoelectric Shells and Plates. CRC Press.
Schulze, S., Pander, M., Naumenko, K., Altenbach, H., 2012. Analysis of laminated glass beams for photovoltaic applications. Int. J. Solids Struct. 49 (15–16), 2027–2036.
Singh, P., Sheikh, J., Behera, B.K., 2024. Metal-faced sandwich composite panels: A review. Thin-Walled Struct. 195, 111376.
Smyczynski, M.J., Magnucka-Blandzi, E., 2018. The three-point bending of a sandwich beam with two binding layers–comparison of two nonlinear hypotheses. Compos. Struct. 183, 96–102.
Tuwair, H., Volz, J., ElGawady, M.A., Chandrashekhara, K., Birman, V., 2016. Modeling and analysis of GFRP bridge deck panels filled with polyurethane foam. J. Bridg. Eng. 21 (5), 04016012.
Vinson, J.R., 2018. The Behavior of Sandwich Structures of Isotropic and Composite Materials. Routledge.
Wijeyewickrema, A.C., Horgan, C.O., Dundurs, J., 1996. Further analysis of end effects for plane deformations of sandwich strips. Int. J. Solids Struct. 33 (29), 4327–4336.
Wilde, M.V., Surova, M.Y., Sergeeva, N.V., 2022. Asymptotically correct boundary conditions for the higher-order theory of plate bending. Math. Mech. Solids 27 (9), 1813–1854.
Yuan, C., Bergsma, O., Koussios, S., Zu, L., Beukers, A., 2012. Optimization of sandwich composites fuselages under flight loads. Appl. Compos. Mater. 19 (1), 47–64.
Zhuang, W., Yang, C., Wu, Z., 2021. Aeroelastic analysis of foam-filled composite corrugated sandwich plates using a higher-order layerwise model. Compos. Struct. 257, 112996.